The formin FMNL3 assembles plasma membrane protrusions that participate in cell–cell adhesion

Timothy J. Gauvin, Lorna E. Young, and Henry N. Higgs
Department of Biochemistry, Geisel School of Medicine at Dartmouth, Hanover, NH 03755

ABSTRACT **FMNL3 is a vertebrate-specific formin protein previously shown to play a role in angiogenesis and cell migration. Here we define the cellular localization of endogenous FMNL3, the dynamics of GFP-tagged FMNL3 during cell migration, and the effects of FMNL3 suppression in mammalian culture cells. The majority of FMNL3 localizes in a punctate pattern, with >95% of these puncta being indistinguishable from the plasma membrane by fluorescence microscopy. A small number of dynamic cytoplasmic FMNL3 patches also exist, which enrich near cell–cell contact sites and fuse with the plasma membrane at these sites. These cytoplasmic puncta appear to be part of larger membranes of endocytic origin. On the plasma membrane, FMNL3 enriches particularly in filopodia and membrane ruffles and at nascent cell–cell adhesions. FMNL3-containing filopodia occur both at the cell–substratum interface and at cell–cell contacts, with the latter being 10-fold more stable. FMNL3 suppression by siRNA has two major effects: decrease in filopodia and compromised cell–cell adhesion in cells migrating as a sheet. Overall our results suggest that FMNL3 functions in assembly of actin-based protrusions that are specialized for cell–cell adhesion.**

Monitoring Editor
Thomas D. Pollard
Yale University

Received: Jul 30, 2014
Revised: Nov 12, 2014
Accepted: Nov 18, 2014

INTRODUCTION

Formins are actin polymerization factors, and the large number of mammalian formins (15 distinct genes) suggests a wide range of cellular functions (Higgs and Peterson, 2005; Campellone and Welch, 2010). However, precise cellular function is poorly understood for many mammalian formins, as opposed to our much better understanding of formin function in budding or fission yeast (Moseley and Goode, 2006; Kovar *et al.*, 2011). Part of the challenge to elucidation of mammalian formin function is the diversity of mammalian actin-based structures, which are often spatially and structurally interrelated.

The FMNL subfamily of formins (also called FRL formins; Higgs and Peterson, 2005) is metazoan specific, not being found in yeasts or plants. Whereas *Drosophila* and *Caenorhabditis elegans* contain one FMNL, vertebrates contain three genes: FMNL1, FMNL2, and FMNL3. Each vertebrate FMNL possesses at least two splice variants. As with other formins, FMNLs are modular (Vaillant *et al.*, 2008; Heimsath and Higgs, 2012), with the following functional regions (Figure 1): GTPase-binding domain (GBD), diaphanous inhibitory domain (DID), dimerization domain (DD), formin homology 1 domain (FH1), formin homology 2 domain (FH2), WH2-like domain (WH2L), and diaphanous autoregulatory domain (DAD). The FH2 domain binds actin- filament barbed ends and can accelerate filament nucleation, as well as regulate filament elongation. In FMNLs, the FH2 has poor actin nucleation activity but can bundle filaments in vitro (Vaillant *et al.*, 2008; Harris *et al.*, 2004, 2010; Block *et al.*, 2012). C-terminal to the FH2 domain, FMNLs contain a WH2-like actin monomer–binding sequence, which is capable of capping barbed ends in isolation or accelerating actin nucleation when coupled to the FH2 domain (Heimsath and Higgs, 2012). Similar to other formins, FMNL regulation is through autoinhibitory interaction of the DID and DAD regions, with activation by Rho GTPase binding to the GBD (Seth *et al.*, 2006; Block *et al.*, 2012). Finally, FMNLs are known or suspected to be N-terminally myristoylated (Han *et al.*, 2009; Block *et al.*, 2012; Moriya *et al.*, 2012), which is a modification not found in other formins.

The cellular functions of FMNLs are incompletely understood. FMNL1 (also called FRL1) has been implicated in diverse functions, including cell migration, phagocytosis, myofibril development, podosome assembly, and centrosome polarization (Seth *et al.*, 2006;

This article was published online ahead of print in MBoC in Press (http://www.molbiolcell.org/cgi/doi/10.1091/mbc.E14-07-1247) on November 26, 2014.

Address correspondence to: Henry N. Higgs (henry.higgs@dartmouth.edu).

Abbreviations used: DAD, diaphanous auto-regulatory domain; DID, diaphanous inhibitory domain; FH1, formin homology domain 1; FH2, formin homology domain 2; GBD, GTPase-binding domain; NC, North Carolina splice variant of FMNL3; PH, Philadelphia splice variant of FMNL3; WGA, wheat germ agglutinin; WH2, WASP homology 2 motif.

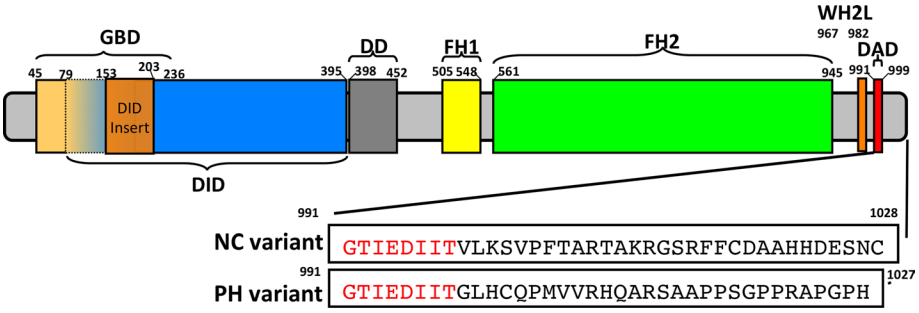

FIGURE 1: FMNL3 domain map and splice variants. DAD, diaphanous autoregulatory domain. DID, diaphanous inhibitory domain; DD, dimerization domain; FH1, formin homology 1 domain; FH2, formin homology 2 domain; GBD, GTPase-binding domain; WH2L, WH2-like domain. Numbers indicate amino acid positions. Splice variants: DID insert (153–203) and alternate C-termini (NC and PH variants, named by the two C-terminal residues). Red letters represent the last common sequence before the alternative splice site. DAD is predicted to extend into the alternately spliced region (with L1000 predicted to make an important interaction with DID).

Gomez *et al.*, 2007; Mersich *et al.*, 2010; Favaro *et al.*, 2013; Naj *et al.*, 2013; Rosado *et al.*, 2014). One FMNL1 splice variant localizes at or near the Golgi and plays a role in Golgi structure and function (Colon-Franco *et al.*, 2011). FMNL2 (also called FRL3) plays a role in cell migration (Block *et al.*, 2012) and appears to be particularly important in metastasis of certain cancers (Zhu *et al.*, 2008, 2011; Kitzing *et al.*, 2010; Li *et al.*, 2010; Liang *et al.*, 2013). In mouse melanoma cells, FMNL2 localizes to the leading-edge plasma membrane, where it appears to promote lamellipodial extension by allowing elongation of Arp2/3 complex–nucleated filaments (Block *et al.*, 2012).

The cellular functions of FMNL3 (also called FRL2) are less defined than those of FMNL1 or FMNL2. FMNL3 plays a role in angiogenesis in zebrafish (Hetheridge *et al.*, 2012). In PC3 prostate cancer cells, which migrate as single cells, FMNL3 depletion inhibits cell migration (Bai *et al.*, 2011; Vega *et al.*, 2011). However, there is little information on what types of actin-based structure are promoted by FMNL3 (filopodia, lamellipodia, etc) and no information as to FMNL3's localization. A previous study in our laboratory showed that overexpression of minimal FMNL3 constructs (containing FH1 and FH2 domains) potently induced filopodia, whereas a similar construct of FMNL1 did not (Harris *et al.*, 2010), but this result does not speak to the function of the endogenous protein.

In this work, we examine the location, dynamics, and function of FMNL3 in adherent culture cells (U2OS and 3T3). We show that the majority of FMNL3 localizes in a punctate pattern at the plasma membrane, with particular enrichment at filopodia, ruffles, and cell–cell adhesions. A small pool of intracellular FMNL3 is present as dynamic puncta that enrich near cell–cell adhesion sites and are associated with larger internal membrane structures. FMNL3 suppression decreases both filopodial number and stability at the leading edge, as well as the integrity of cell–cell contacts.

RESULTS

FMNL3 localizes in a punctate pattern that enriches at the leading edge and cell–cell contacts

As a first step in determining FMNL3 function, we examined localization of the endogenous protein in U2OS human osteosarcoma cells (Figure 2) and NIH 3T3 mouse fibroblasts (Supplemental Figure S1) by immunofluorescence microscopy, using an affinity-purified antibody against the FH2 domain. The specificity of this antibody for FMNL3 is indicated by the effect of small interfering RNA (siRNA) suppression, which removes all of the peripheral immunofluorescence staining, leaving a hazy perinuclear staining that we interpret as nonspecific background (see later discussion of Figure 7D and Supplemental Figure S6B). We focus on the peripheral, siRNA-sensitive stained regions.

FMNL3 mostly appears as punctate staining, with puncta diameters close to the limit of resolution (370 ± 50 nm, n = 82; Figure 2D). In cells plated on glass overnight, these puncta are present throughout the cell but enrich at areas of apparent membrane protrusion (Figure 2A and Supplemental Figure S1A). This enrichment is observed most easily when cells are induced to spread upon replating. U2OS cells spread asymmetrically on laminin, allowing clear observation of the FMNL3-rich spreading edge as opposed to the FMNL3-poor nonspreading edge (Figure 2B). In addition, short filopodia are visible at the spreading edges of U2OS cells on laminin, and FMNL3 is enriched at filopodial tips in these cells (Figure 2B, inset). 3T3 cells plated on poly-L-lysine (PLL) spread uniformly, and FMNL3 enriches significantly at the spreading edge, still in a punctate pattern (Supplemental Figure S1B).

We also examined FMNL3 localization in a wound-healing context in which cells are plated on glass at high density overnight and then scrape-wounded and allowed to migrate into the wound for several hours. Again, FMNL3 enriches at the leading edge during wound closure (Figure 2C and Supplemental Figure S1C), but filopodia are not apparent upon fixation in either 3T3 or U2OS cells (however, see later discussion of evidence that fixation ablates these filopodia, Figure 8). FMNL3 also enriches at some but not all areas of cell–cell contact (Figure 2C and Supplemental Figure S1C). From these results, we conclude that FMNL3 localizes largely to diffraction-limited puncta throughout the cell, with particular enrichment at areas of active cell protrusion or cell–cell contacts.

We further investigated FMNL3 enrichment to actively protruding regions of the plasma membrane using serum readdition after serum starvation of NIH 3T3 cells. The most intense FMNL3 enrichment is to areas of cell–cell contact, with clear enrichment within 10 min (Figure 3). N-cadherin, the predominant cadherin in 3T3 cells, enriches at contact sites on a similar time scale (Figure 3). At early time points after serum readdition, the FMNL3/N-cadherin enrichment resembles interdigitating filopodia, similar to observations made in other systems (Adams *et al.*, 1998; Vasioukhin *et al.*, 2000; Brevier *et al.*, 2008; Hoelzle and Svitkina, 2012). Later in the process, the contact site becomes compact, and the filopodia are no longer evident.

Live-cell analysis of FMNL3 localization and dynamics

The preceding experiments were conducted using immunofluorescence detection of endogenous FMNL3. To analyze FMNL3 dynamics, we developed a green fluorescent protein (GFP)–fusion protein. It is worth mentioning that several challenges presented themselves during this development. First, there are two known alternatively spliced sites for FMNL3: a variably present 51–amino acid insert in the DID, and alternate C-termini of 30 or 29 amino acids (Figure 1). We determined that U2OS cells expressed the variant containing the DID insert and the NC C-terminus (Supplemental Figure S2) and used this variant (called "NC") henceforth. Second, we found that placing the GFP at either the N- or C-terminus caused localization patterns that were clearly different from that of endogenous FMNL3, with GFP-FMNL3 localization being entirely internal and FMNL3-GFP being entirely on the plasma membrane and causing a significant increase

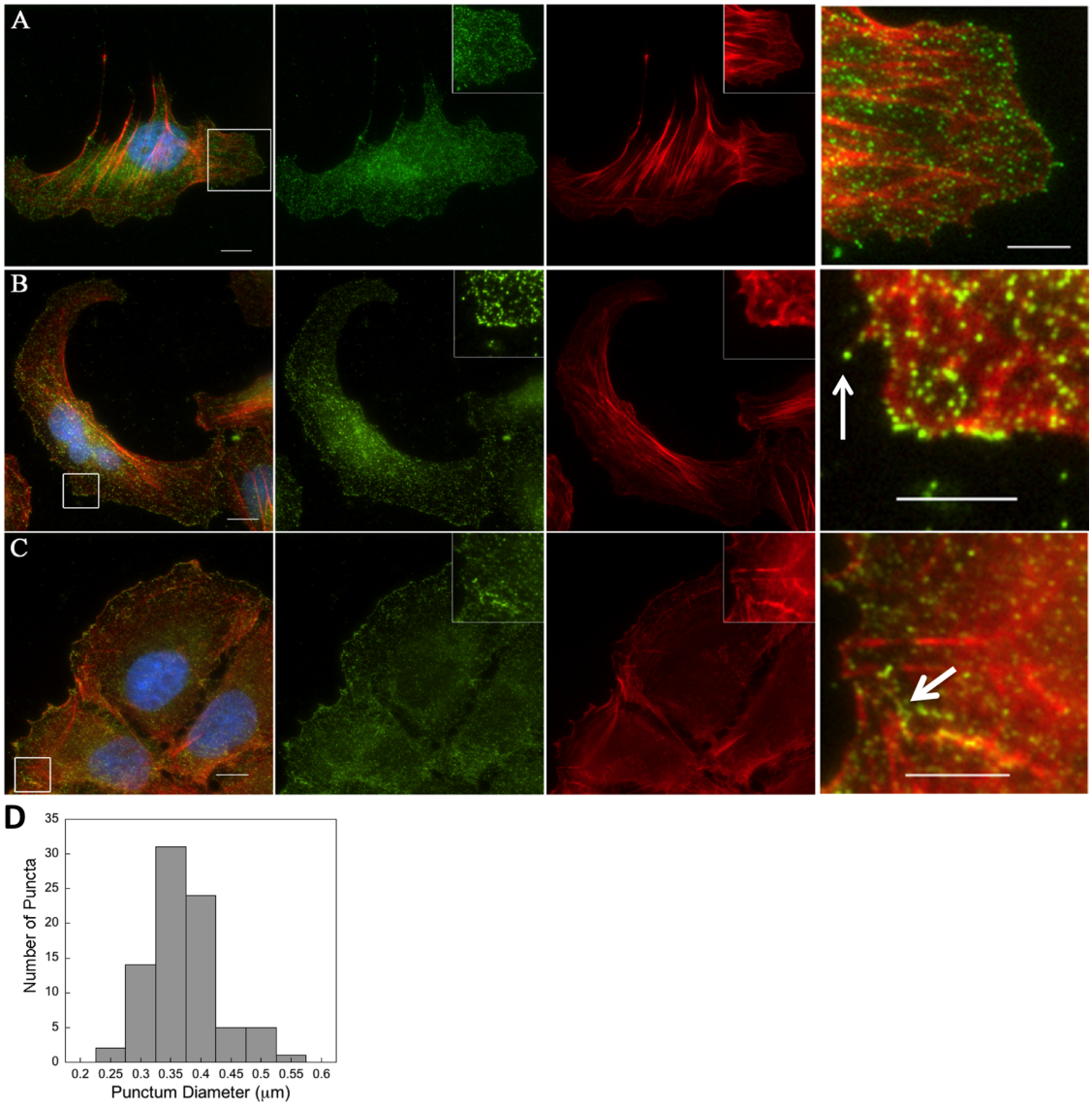

FIGURE 2: Localization of FMNL3 in U2OS cells. U2OS cells were examined in three conditions: (A) plated on glass coverslips overnight, (B) plated on laminin coated slips for 120 min, and (C) during wound-healing assay, 23 h after wounding. Stains are anti-FMNL3 antibody (green), phalloidin for actin filaments (red), and DAPI for DNA (blue). Right, zooms. Arrow in B indicates a filopodium, and arrow in C indicates region of cell–cell contact, which runs diagonally from this arrow to the lower right corner. Scale bars,10 μm (full images), 5 μm (zooms). (D) Histogram of FMNL3 puncta diameters from images of fixed U2OS cells stained with anti-FMNL3 antibodies. Bins are 50 nm, bars are centered at the maximum value of that bin (e.g., bar centered on 350 nm represents 300–350 nm). Similar to images for NIH 3T3 cells shown in Supplemental Figure S1.

in filopodia (Supplemental Figure S3). For this reason, we developed a construct in which the GFP was placed at the N-terminal end of the FH1 domain (construct called the FMNL3-NC-GFPint), which is a region predicted to adopt a nonfolded structure (Paul and Pollard, 2009; Courtemanche and Pollard, 2012). FMNL3-NC-GFPint produces a pattern more similar to endogenous FMNL3 in fixed cells, both at leading edge and puncta (Supplemental Figure S3). Third, we were unable to generate stable cell lines constitutively expressing FMNL3-NC-GFPint from a cytomegalovirus promoter. For this reason, we developed a stable doxycycline-inducible FMNL3-NC-GFPint line in U2OS cells, which displays low-level expression after 18–24 h of induction. Quantification of GFP-FMNL3 and total FMNL3 levels suggests that FMNL3-NC-GFPint levels are significantly less than endogenous FMNL3 levels in all cells examined (Supplemental Figure S4).

Using this cell line, we first examined localization of FMNL3 puncta in more detail. Our initial laser-scanning confocal microscopy analysis of fixed cells stained for endogenous FMNL3 suggested that FMNL3 puncta were predominately at/near the plasma membrane (PM; Figure 4A), but the flattening that occurred upon cell fixation/permeabilization rendered interpretation of these data challenging. Similar three-dimensional (3D) reconstructions of live U2OS cells expressing FMNL3-NC-GFPint provide a much less ambiguous result. As a marker for both the plasma membrane and internal membranes, we used fluorescent wheat germ agglutinin (WGA), which binds *N*-acetyl-glucosamine and sialic acid moieties on the cell surface and gets rapidly endocytosed (Raub *et al.*, 1990). Immediately after WGA treatment, the vast majority of FMNL3 puncta reside at positions indistinguishable from the PM (Figure 4B and Supplemental Movies S1

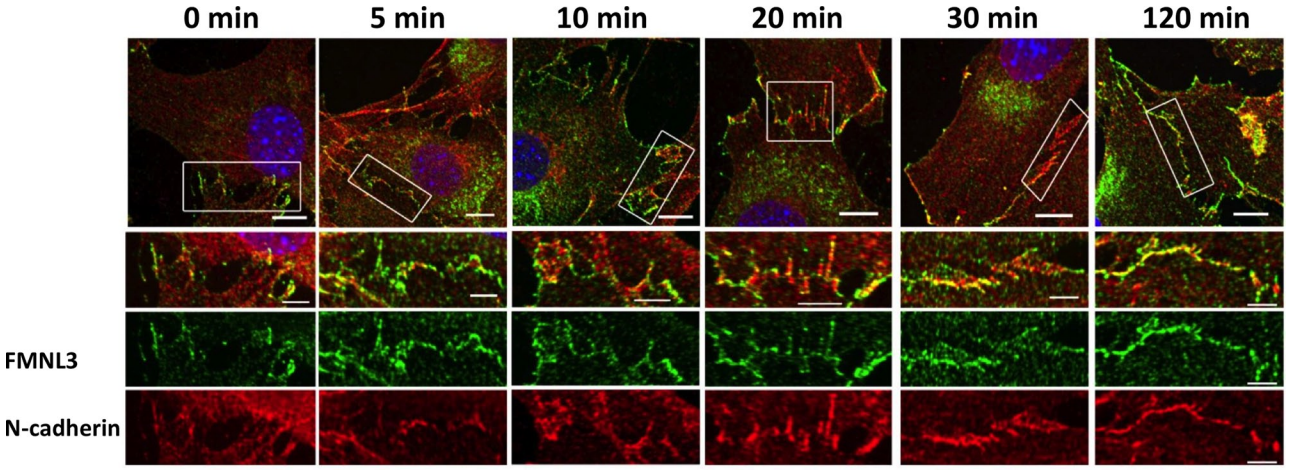

FIGURE 3: FMNL3 translocates to nascent cell–cell junctions upon serum addition. Serum-starved NIH 3T3 cells were treated with serum-containing medium (10% newborn calf serum) for the indicated times and then fixed and stained for FMNL3 (green), N-cadherin (red), and DNA (blue). Scale bar, 10 μm (close-ups, 5 μm).

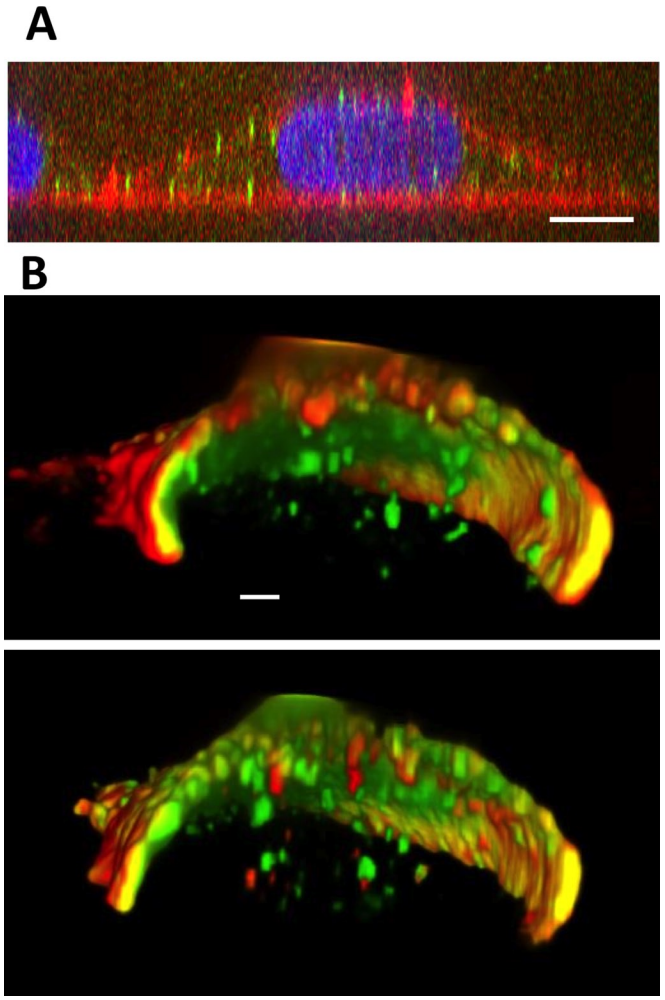

FIGURE 4: Localization of FMNL3 puncta. (A) *XZ*-projection of fixed U2OS cells immunostained for endogenous FMNL3 (green), plasma membrane (red), and DNA (blue), then imaged by laser scanning confocal microscopy using 100-nm *Z*-slices. Plasma membrane labeled with FM4-64 (50 μM in Hank's buffered salt solution) for 1 min before fixation. *XZ*-projection reconstructed using Nikon Elements software with 2× scale of *Z*-axis. Scale bar, 10 μm (*XY*), 5 μm (*Z*). (B) A 3D reconstruction of FMNL3-NC-GFPint (green) and Alexa 647–labeled WGA (red) in live U2OS cell at <1 min after WGA treatment (top) and at 5 min after treatment (bottom). The *Z*-stack was deconvolved before assembling the 3D image. Scale bar, 2 μm (*XY*), 1 μm (*Z*). See corresponding Supplemental Movies S1 and S2.

and S2), with <5% of the puncta being clearly separate from the PM (three cells counted, 14/280, 17/476, and 17/586 internal puncta/total puncta, respectively). As opposed to the spherical structures observed by fixed-cell immunofluorescence, the surface FMNL3 staining observed in 3D reconstruction images of FMNL3-NC-GFPint is more oblate and somewhat interconnected.

The cytoplasmic FMNL3 puncta are rapidly motile in the vicinity of the FMNL3-enriched cell–cell contact, with some undergoing random movement and others moving directionally (Figure 5, A and B, and Supplemental Movie S3). Occasionally, the puncta move to and fuse with the plasma membrane (Supplemental Movie S2). We observe no LifeAct enrichment around these puncta (unpublished data), suggesting that their dynamics is actin-independent. When cells are treated with WGA for longer times to label endocytic compartments, subpopulations of cytoplasmic FMNL3 and WGA structures colocalize in an intriguing manner. The cytoplasmic FMNL3 puncta appear as diffraction-limited spheres that are clearly associated with the larger WGA-labeled structures (Figure 5, C and D). Both the FMNL3 and associated WGA structures can move rapidly in the cytoplasm (Figure 5D and Supplemental Movie S4).

Next we examined the dynamics of FMNL3-NC-GFPint at the cell surface. On the basal surface, FMNL3 puncta are relatively static, showing little change in movement over several minutes (Figure 6A). The apical puncta are difficult to track because of the rapid changes in the surface in general. Near protrusive regions, however, FMNL3 displays an association with membrane ruffles that are also enriched in actin, as detected by LifeAct (Figure 6B and Supplemental Movie S5) or mCherry-actin (Supplemental Figure S5). These ruffles are highly dynamic but do not move consistently in a retrograde manner (Figure 6C and Supplemental Movie S5). The ruffles also stain brightly with WGA, and the dynamics of the WGA stain overlaps the dynamics of FMNL3 in the ruffles (Figure 6, B and C). Treatment with latrunculin B causes dissipation of both FMNL3 and actin signals within 2 min (Supplemental Figure S5).

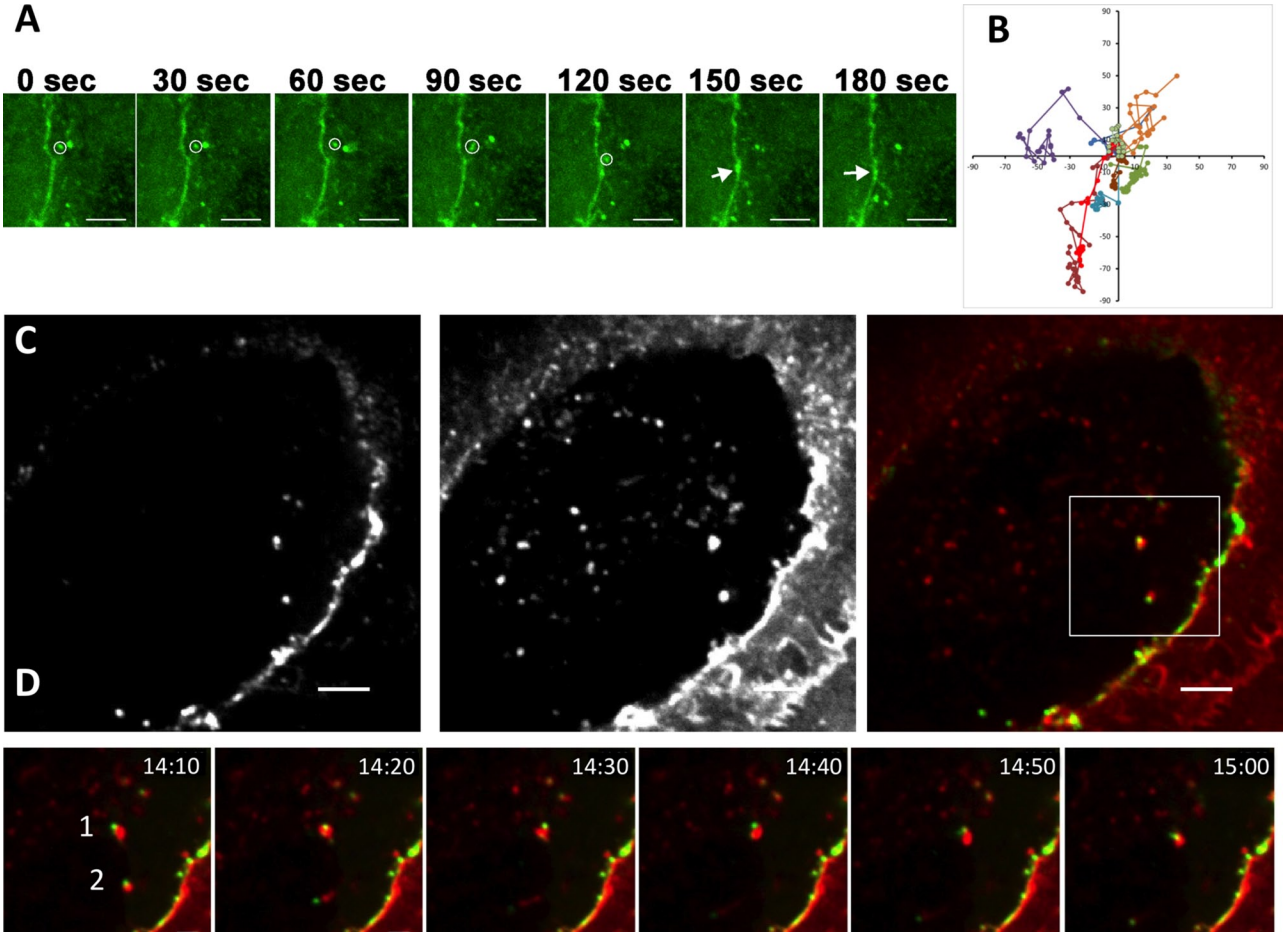

FIGURE 5: Dynamics of cytoplasmic FMNL3 puncta near cell–cell contact sites. (A) Individual time points from Supplemental Movie S2, following cytoplasmic FMNL3-NC-GFPint puncta near the cell–cell contact. Note the circled punctum, which has recently undergone fission from the larger punctum and fuses with the plasma membrane (arrow). Scale bar, 5 μm. See corresponding Supplemental Movie S3. (B) Trajectory plots for individual intracellular puncta, with the origin representing the starting position for each punctum. Units are in pixels, 0.151 μm/pixel. (C) Single time frame (14 min) from live-cell recording, showing FMNL3-NC-GFPint (green) and Alexa 647–WGA (red) after >10 min of WGA treatment, which allows time for endocytic uptake of WGA. Individual FMNL3 (left) and WGA (center) are also shown in black and white. Box indicates approximate region shown in D and Supplemental Movie S4. Scale bar, 5 μm. (D) Montage taken from Supplemental Movie S4, showing FMNL3-NC-GFPint (green) and WGA (red) dynamics over 50-s period (individual frames represent 10-s intervals). Two WGA-containing particles are labeled. Particle 1 is relatively static over this time period, whereas particle 2 moves rapidly, becoming dimmer but still distinguishable during the process. See also Supplemental Movie S4 from 14:10 to 15:00. Scale bar, 2 μm.

FMNL3 also enriches in filopodia, both at protrusive edges and at cell–cell contacts (Figure 6D). The stability of filopodia at these two locations differs greatly, with protrusive-edge filopodia having much shorter lifetimes (median 2.5 ± 1.7 min) than cell-cell–contact filopodia (median 25 ± 6.5 min), with many contact filopodia being stable throughout the 27-min viewing period (Figure 6, D and E, and Supplemental Movies S6 and S7). The cell–cell contact protrusions appear to be bona fide filopodia and not retraction fibers because the majority exhibits clear growth during observation time and are not under any apparent tension (Supplemental Movie S7). We note that the FMNL3 features observed here (surface puncta, cytoplasmic puncta, ruffles, and filopodia) are not dependent on WGA treatment (unpublished data).

FMNL3 suppression results in loss of leading-edge filopodia and unstable cell–cell contacts

We used siRNA-mediated suppression to examine the importance of FMNL3 to cellular dynamics, focusing on U2OS cells due to the ability to attain >85% suppression levels (Figure 7, A and B). FMNL3 suppression also reduces by >80% the number of puncta observed using the anti-FMNL3 antibody (Figure 7, C and D), suggesting that these puncta do indeed correspond to FMNL3. A similar reduction in anti-FMNL3–stained puncta occurs upon FMNL3 suppression in 3T3 cells (Supplemental Figure S6).

FMNL3 suppression does not have a strong effect on spreading rate for U2OS on laminin or 3T3 cells on PLL (unpublished data), nor does FMNL3 suppression affect wound closure rate in the wound-healing assay (Supplemental Figure S7, A and B). However, FMNL3 suppression does compromise filopodial abundance during both spreading and wound healing. In U2OS cells spreading on laminin, filopodial density decreases by >50% upon FMNL3 suppression (Figure 7, E and F). In live-cell analysis of wound healing, we detect abundant and highly dynamic filopodia at the leading edges of control wound-edge cells, with lifetimes of 116 ± 56 s (Figure 8A and Supplemental Movie S8). FMNL3 suppression causes a 3.4-fold reduction in filopodial number and a significant decrease in the

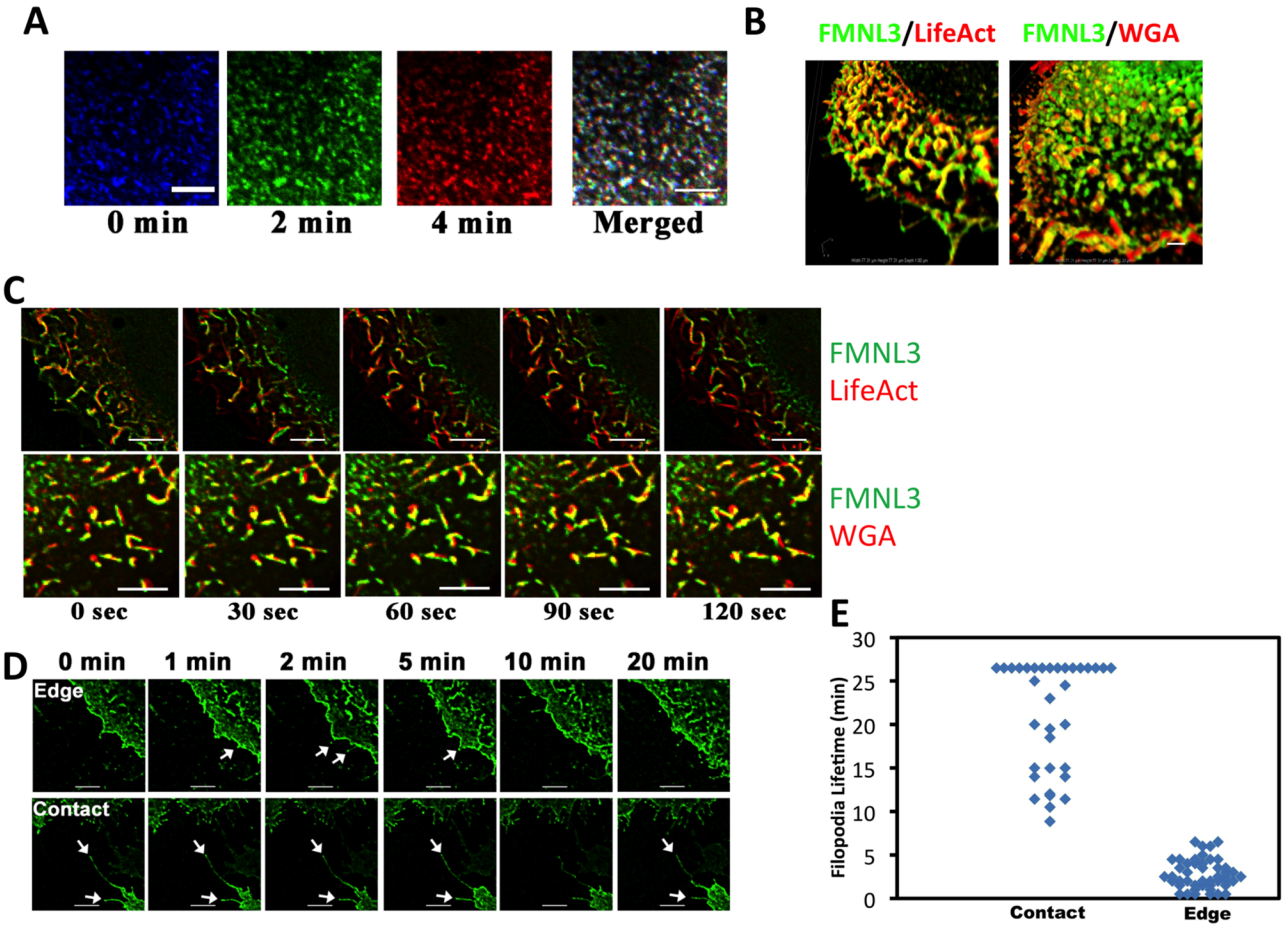

FIGURE 6: Dynamics of FMNL3 in basal puncta, membrane ruffles, and filopodia. All images use U2OS cells expressing FMNL3-NC-GFPint. (A) Three frames of a time-lapse movie examining FMNL3 on the basal surface, with the overlay of the three frames on the right. In the overlay, note the preponderance of white puncta, indicating that they did not displace significantly over the 4-min viewing time. Scale bar, 5 μm. (B) 3D reconstructions of protrusive regions, with FMNL3 in green and either LifeAct (left) or WGA (right) in red. Ruffles protrude above the apical cell surface. (C) Individual frames from time-lapse movies, tracking FMNL3 and either LifeAct (top) or WGA (bottom). Scale bar, 5 μm. Corresponds to Supplemental Movie S5 (LifeAct). (D) Individual frames from time-lapse movies following FMNL3 in filopodia at a free cell edge ("edge," top) or a cell edge that is in contact with another cell ("contact," bottom). In the latter case, the cell being contacted is not expressing FMNL3 (and is invisible here but visible by DIC microscopy). Scale bar, 5 μm. Corresponds to Supplemental Movies S6 and S7. (E) Filopodia lifetimes for contact and edge filopodia, measured from five cells. A substantial proportion of contact filopodia were present for the entire recorded time (27 min).

lifetimes of the remaining filopodia (70.6 ± 37 s; Figure 8, A–C, and Supplemental Movie S9). The presence of leading-edge filopodia in our live-cell imaging of wound healing contrasts with our finding of few filopodia in fixed cells under the same conditions (Figure 2C), suggesting that formaldehyde fixation destroys these transient structures.

Because FMNL3 enriches at cell–cell contacts, we analyzed the effects of FMNL3 suppression on the stability of cell–cell contacts during wound healing. Control U2OS cells migrate as a sheet, with few gaps between cells (Figure 9A). In fixed-cell assays, the area of these gaps increases >2.5-fold upon FMNL3 suppression (Figure 9B). In live-cell imaging, control cells maintain tight contact, and any small gaps close rapidly (Figure 9C and Supplemental Movie S10). In contrast, FMNL3-suppressed cells display frequent gaps between cells, and these gaps close approximately threefold more slowly (Figure 9, C and D, and Supplemental Movie S11). Gaps appear to result from the reduced ability of neighboring cells to maintain stable interaction upon contact, suggesting that FMNL3 suppression results in decreased cell–cell adhesion.

DISCUSSION

In this article, we show that FMNL3 localizes in a punctate pattern in U2OS and 3T3 cells, with >95% of these puncta being at or near the plasma membrane. Further enrichment occurs in several places: at the leading-edge plasma membrane, particularly at filopodial tips; at the ridges of apical membrane ruffles; and at cell–cell contact sites. The relatively infrequent cytoplasmic FMNL3 puncta are dynamic and can fuse with the plasma membrane at cell–cell contact sites. Suppression of FMNL3 by siRNA causes a reduction in filopodia at the leading edge and in cell–cell adhesion for U2OS cells migrating as a sheet in wound-healing assays.

The identity of the abundant FMNL3 puncta found at the cell surface is intriguing. From 3D reconstructions of cells expressing the GFP-FMNL3 construct, we find 300–600 surface puncta, all at or near the diffraction limit. At the level of light microscopy, we cannot determine whether these puncta represent vesicles that are closely associated with the plasma membrane (akin to secretory vesicles) or are actually regions of FMNL3 enrichment on the plasma

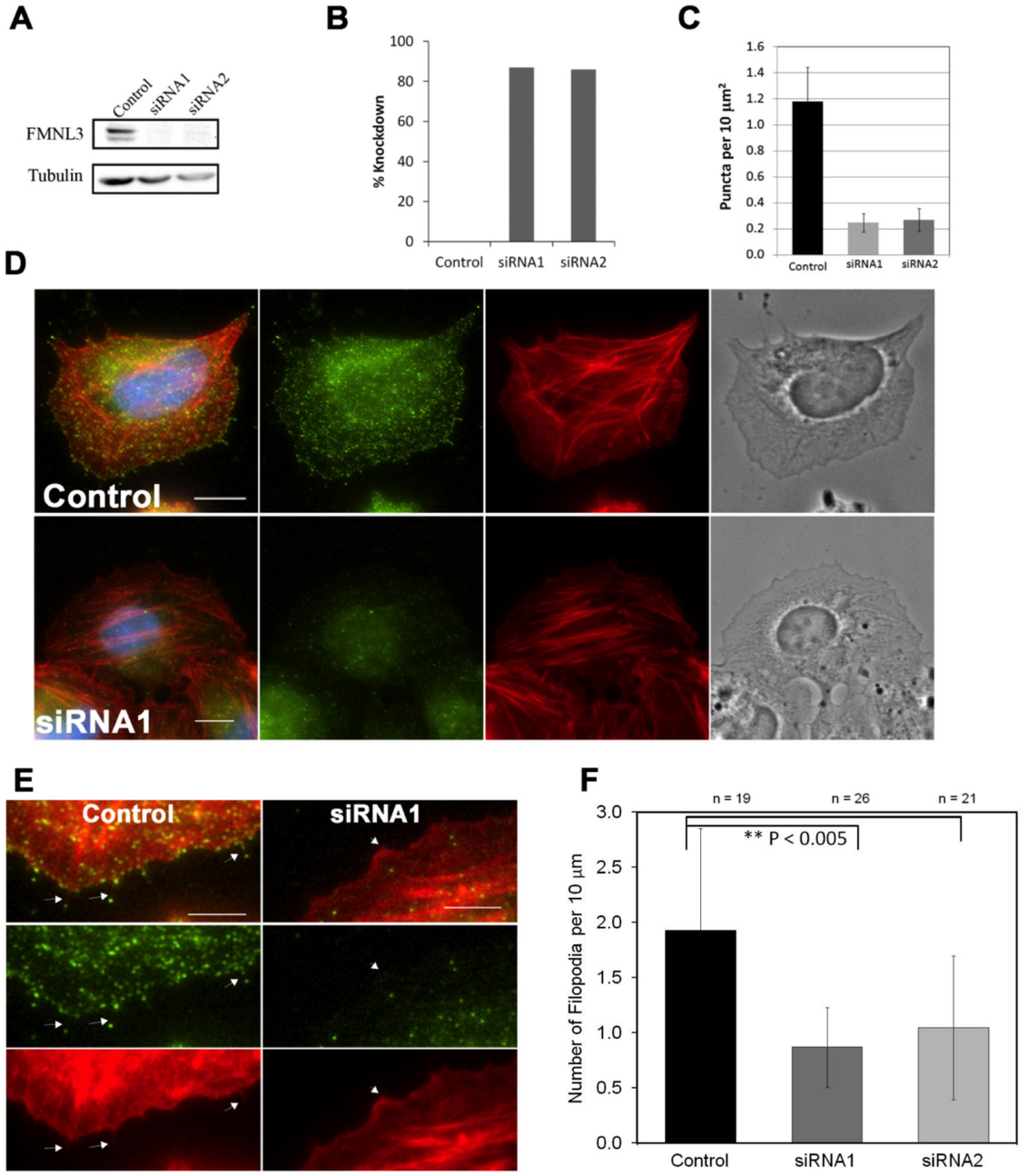

FIGURE 7: Effects of FMNL3 suppression in U2OS cells. (A) Western blot showing suppression of FMNL3 using two different siRNAs. (B) Percentage suppression, determined by density measurements from Western blots. (C) Quantification of average puncta per 10 µm^2 area in control and FMNL3-depleted cells. Error bars represent SD. (D) Cells plated on laminin-coated coverslips for 90 min for control (top) and siRNA1 treatment (bottom). Stains were for FMNL3 (green), actin filaments (red), and DNA (blue). Scale bar, 10 µm. (E) Close-ups of spreading edge in control (left) siRNA knockdown (right column) shows decrease of filopodia present along the edge compared with control (left column). Filopodia indicated with arrows. Scale bar, 5 µm. (F) Graph quantifying filopodia density as filopodia per 10-µm length along the spreading edge. Error bars indicate SD; $p < 0.001$.

membrane, representing lateral segregation ("domains"). Either possibility is intriguing functionally.

The relatively sparse cytoplasmic FMNL3 puncta display interesting features. First, they enrich near cell–cell contact sites, as opposed to a noncontacting region of the cell. Second, they are dynamic and can translocate to the cell–cell contact site, where they fuse with the plasma membrane. Third, the puncta are associated with larger membrane structures derived from endocytosis. These features suggest that the cytoplasmic puncta might be components of dynamic internal membranes that are delivering components to the contact site. There is ample evidence for recycling of adhesion components at cell–cell contact sites (Le *et al.*, 1999; Akhtar and Hotchin, 2001; Palacios *et al.*, 2005; Desclozeaux *et al.*, 2008; Peglion *et al.*, 2014), and FMNL3 could be either part of this recycling system or one of the components that is recycled. The discrete enrichment of FMNL3 puncta to specific regions of these internal membranes is intriguing and could suggest confinement on associated small vesicles or

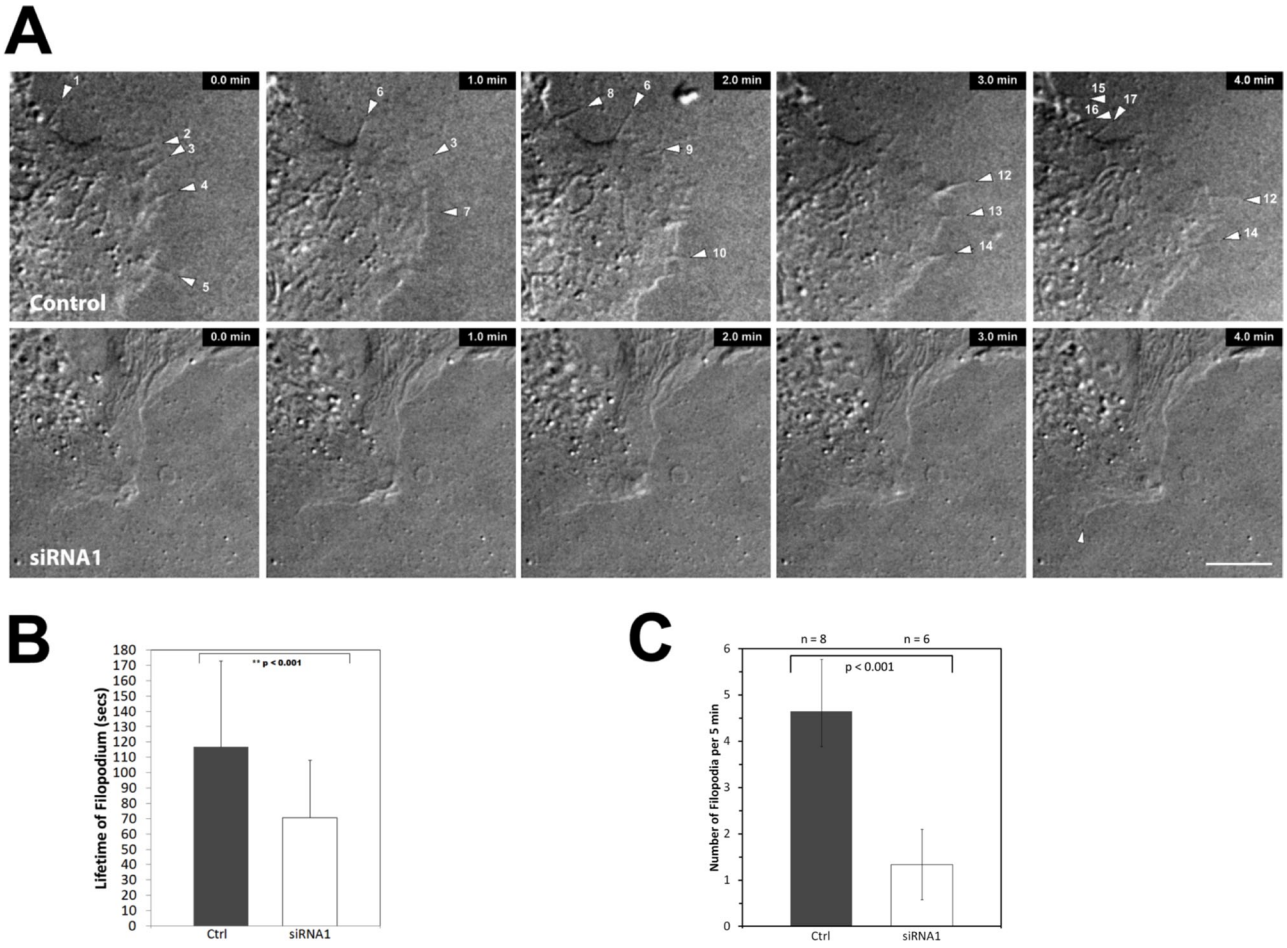

FIGURE 8: FMNL3 suppression reduces filopodial number and lifetime at leading edge of U2OS cells in wound-healing assays. (A) Time-lapse montage of DIC images of leading edge of cells in control and knockdown cells. Arrows indicate filopodia. Scale bar, 10 μm. Corresponds to Supplemental Movies S8 and S9. (B) Quantification of average filopodium lifetime. Error bars indicate SD. (C) Quantification of filopodia assembly frequency. Error bars indicate SD.

possibly membrane segregation on the endosomal membrane (Trajkovic *et al.*, 2008).

The finding that FMNL3 enriches in filopodia, as well as the effect of FMNL3 suppression on filopodial abundance, extends our previous observation that minimal constructs of FMNL3 (containing the FH1 and FH2 domains) are capable of filopodial induction (Harris *et al.*, 2010). Our work here shows that filopodial assembly is a bona fide function of FMNL3, as opposed to a potentially artifactual effect of the FH1-FH2 construct. FMNL3-assembled filopodia might be specialized for cell–cell adhesion, based on two observations: the filopodia are 10-fold more stable when in contact with another cell, and FMNL3 suppression causes defects in cell–cell adhesion. Filopodia clearly play a role in cadherin-mediated cell–cell adhesion in both epithelial (Adams *et al.*, 1998; Vasioukhin *et al.*, 2000; Brevier *et al.*, 2008) and endothelial cells (Hoelzle and Svitkina, 2012), and our work here shows that N-cadherin enriches with FMNL3 at cell–cell contacts. It will be interesting to determine whether FMNL3-induced filopodia preferentially enrich cell–cell adhesion molecules.

The difficulty experienced in producing a GFP-tagged FMNL3 construct that suitably mimics endogenous FMNL3 localization might be an indication of peculiarities in FMNL3 regulation. N-terminally tagged FMNL3 did not localize to the plasma membrane but instead to intracellular aggregates, which might not be surprising, given the N-terminal myristoylation site that was ablated by the tag (Han *et al.*, 2009; Block *et al.*, 2012; Moriya *et al.*, 2012). Of greater interest, C-terminally tagged FMNL3 appeared "constitutively active," localizing intensely to the plasma membrane and causing a significant increase in filopodia. This result suggests that the extreme C-terminus influences FMNL3 regulation and might relate to previous findings showing FMNL3 to be less tightly regulated than FMNL2 (Vaillant *et al.*, 2008) and mDia2 (Harris *et al.*, 2010).

It is interesting that our study finds no defect in cell migration upon FMNL3 suppression, whereas a previous study did identify a migration defect (Bai *et al.*, 2011). A major difference in the two studies is the cell lines used. In our study, we used U2OS and 3T3 cells, both of which display strong cell–cell adhesion and migrate as a sheet in wound-healing assays. The previous study used PC3 human prostate cancer cells, which display weak cell–cell adhesion and migrate as single cells in wound-healing assays. One possibility is that FMNL3's role is cell-type dependent, participating predominantly in cell–cell adhesion in adhesive cell lines and participating more in cell migration in less adhesive cells. In any case, it is clear that FMNL3, like the other vertebrate FMNLs, has several cellular roles, so the elucidation of these roles is likely to produce new surprises in the future.

MATERIALS AND METHODS

Cell lines and culture conditions

U2OS (human osteosarcoma, originally from Duane Compton, Dartmouth, Hanover, NH) and NIH 3T3 cells (originally from

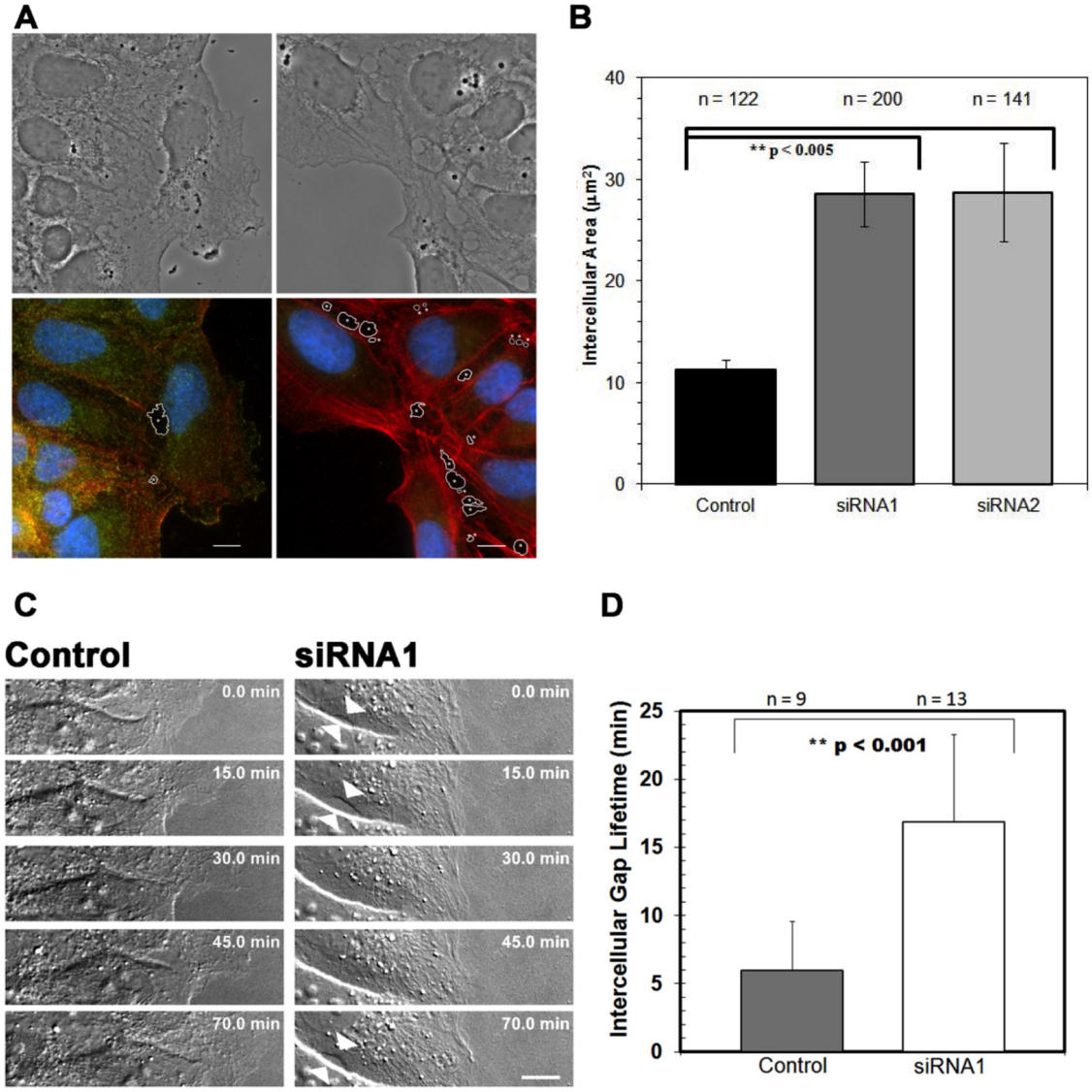

FIGURE 9: FMNL3 suppression increases intercellular gaps between U2OS cells in wound- healing assays. (A) Phase-contrast (top) and merged fluorescence images (bottom) of FMNL3 (green), actin (red), and DNA (blue) along wound edge of control (left) and siRNA1-treated cells (right) show an increase of intercellular gaps (marked by asterisks) upon FMNL3 depletion. Scale bars, 10 µm. Corresponds to Supplemental Movies S10 and S11. (B) Graph shows average areas of intercellular spaces. Error bars show SEM; $p < 0.005$. (C) DIC time-lapse montage of wound edge in control and knockdown cells. Arrows indicate intercellular gaps forming during time lapse. Scale bar indicates 10 µm. (D) Average lifetime of intercellular gaps during wound healing. Error bars indicate SD.

Gregg Gundersen, Columbia University, New York) were cultured in DMEM (Corning, Corning, NY) and 10% newborn calf serum (Altanta Biologicals, Flowery Branch, GA) at 37°C and 5% CO_2. For U2OS cell lines transfected with the pTet-on Advance plasmid (Clontech, Mountain View, CA) and U2OS Tet-on FMNL3-NC-GFPint construct, the serum used was 10% Tet-approved fetal bovine serum (Clontech). To induce expression of FMNL3-NC GFPint, cells were incubated in 1 µg/ml doxycycline (Fisher Scientific, Pittsburgh, PA) for 18–24 h before imaging.

Plasmids and siRNA constructs

All FMNL3 constructs were created from a human FMNL3 open reading frame (ORF) containing the DID insert and the PH C-terminal splice variant (Figure 1), a kind gift from John Copeland (University of Ottawa, Canada). To generate the NC variant, the NC C-terminus was amplified by 23°C PCR from U2OS cell cDNA, using primers containing *Kpn*1 and *Eco*R1 sites, and ligated with the rest of the FMNL3 ORF into the pcDNA3.1 vector (Invitrogen, Waltham, MA). All enhanced GFP constructs used were the A206K mutant (low dimerization affinity; Zacharias *et al.*, 2002). The FMNL3-GFP and GFP-FMNL3 constructs were in the pEGFP-N1 and pEGFP-C1 vectors, respectively (Clontech). The FMNL3-NC-GFPint construct was made in the pcDNA3.1 vector by digesting with *Bsu*36i and inserting an amplified GFP construct containing a flexible GSG linker and *Bsu*36i sites on both ends. The GFP construct is inserted at amino acids 512–513 in the FMNL3 sequence (Supplemental Figure S4). The FMNL3-NC GFPint was moved from pcDNA3.1 to pTRE-tight (Clontech) for Tet-on system using *Eco*R1/*Not*I restriction sites. FMNL3-GFP was cloned in the pGFP-N1 vector with *Bam*H1 sites, and the GFP-FMNL3 construct was cloned into GFP-C1 vector using *Bam*H1 sites. siRNA constructs were purchased from Life Technologies (Carlsbad, CA)

(siRNA1, CAUUCGUUCUUACAAGGAA; siRNA 2, GCAUCAAGGAGACAUAUGA). Scrambled siRNA was purchased from Integrated DNA Technologies (Negative Control #1).

For production of the stable FMNL3-NC-GFPint cell line, U2OS stably expressing pTet-on Advance (gift from Bernardo Orr [Dartmouth] and Duane Compton) were transfected with FMNL3-NC GFPint in the pTRE-tight vector (Clontech) using jetPrime (Polypus Transfection). Cells were selected using 0.2 mg/ml G418 in growth medium. Cells were then selected using 0.1 mg/ml hygromycin (Clontech) for 2 wk (to reselect for the pTRE-tight vector) before picking colonies. After selection, colonies were picked, and cells expressing FMNL3-NC-GFPint were screened by anti-FMNL3 Western blotting after inducing each colony with 1 μg/ml doxycycline for 24 h. Pilot experiments showed undetectable expression in the absence of doxycycline (Supplemental Figure S4) and that expression levels were relatively constant from 18 to 30 h postinduction.

Antibodies and other labeling reagents

The anti-FMNL3 antibody was raised in guinea pig (Covance) using the FMNL3-FH1FH2 construct (Harris *et al.*, 2010) as antigen and affinity-purified using this same antigen coupled to sulfolink resin (Thermo Scientific, Waltham, MA). Anti–N-cadherin (mouse, #C3845) and anti-tubulin (mouse, DM1alpha) antibodies were purchased from Sigma-Aldrich (St. Louis, MO). Alexa 488 and Alexa 546–labeled anti–guinea pig secondary antibody and FM4-64 were purchased from Life Technologies. Texas Red–labeled anti-mouse was obtained from Vector Laboratories. Tetramethylrhodamine isothiocyanate (TRITC)–labeled phalloidin was purchased from Sigma-Aldrich. Alexa 647–WGA (Life Technologies) was a kind gift from Brent Berwin (Geisel School of Medicine at Dartmouth).

Cell treatments, fixation, and staining for immunofluorescence

For the spreading assay, 12-mm coverslips were coated overnight with either 0.01% PLL (Sigma-Aldrich) or 20 μg/μl laminin (Sigma-Aldrich). A confluent plate of cells was trypsinized and diluted in phosphate-buffered saline (PBS) before two washes in PBS. Cells were resuspended to 100,000 cells/ml in prewarmed medium before plating 0.5 ml onto coated coverslips. Cells were incubated at 37°C until ready to fix. For serum readdition, NIH 3T3 cells were serum starved by rinsing twice with PBS and incubating in DMEM for at least 20 h. Medium was changed to normal growth medium (10% newborn calf serum) for indicated times before fixation. After treatment, cells were washed once with room temperature PBS, then immediately fixed with 4% paraformaldehyde (Electron Microscopy Sciences, Hatfield, PA) diluted in room temperature PBS for 20 min. Cells were washed and permeabilized with 0.20% Triton X-100 for 20 min at room temperature. Cells were blocked using 10% newborn calf serum diluted in PBS for 1 h at room temperature. Cells were incubated with primary antibodies (FMNL3 1:600, N-cadherin 1:200) diluted in PBS with 1% newborn calf serum for 1 h. Cells were washed, and secondary antibodies diluted 1:500 in PBS were added for 1 h. TRITC–phalloidin was used at 50 nM. Cells were stained with 0.4 ng/μl 4′,6-diamidino-2-phenylindole (DAPI) for 10 min before final rinse with PBS. Cells were mounted to glass slides using PVA-DABCO. Images were acquired using a Nikon TE-2000E microscope with either the 60×/1.4 numerical aperture (NA) or 4×/0.13 NA objective, a Roper CoolSnap camera, and Nikon Elements software.

Wound-healing assays

Cells were plated at high density (310,000 cells on 18-mm coverslips in a 12-well plate) and incubated overnight. Coverslips were assessed for formation of a complete monolayer before making scratches. Scratches were made by attaching a p10 tip to a vacuum manifold set at half strength; a straight line was drawn down the center of the coverslip by holding the tip perpendicular to the coverslip. Wound width was measured at three different spots along the wound from images taken with the 4× objective. For live imaging, cells were incubated for 2 h after making scratches before imaging.

Live-cell microscopy

Coverslips were mounted into modified Rose chambers and then onto a Wave FX spinning disk confocal microscope (Quorum Technologies [Guelph, Canada], on a Nikon Eclipse microscope) with Bionomic Controller (20/20 Technology) temperature-controlled stage set to 37°C. After equilibrating to temperature for 5 min, cells were imaged through the 60×/1.4 NA Plan Apo objective (Nikon USA, Melville, NY) using the 491-nm laser and 525/20 filter for GFP and the 561-nm laser and 593/40 filter for monomeric red fluorescent protein and 655/90 for far red and differential interference contrast (DIC). *Z*-stacks of 0.2 μm were collected for each color at 10- to 30-s intervals. Maximum intensity projections from five *Z*-slices were assembled using Nikon Elements software. For 3D reconstructions of *Z*-stacks of fixed cells, images were deconvolved using Huygens software and reassembled using Nikon Elements. Alexa 647–labeled WGA was resuspended in dimethyl sulfoxide (DMSO) at a concentration of 1 mg/ml, diluted to 500 ng/ml in medium, and added to cells, which were imaged within 1 min to capture the plasma membrane. To observe endocytic compartments, cells were imaged 5–10 min after WGA treatment (endocytic structures were visible within 3 min of treatment). FM4-64 was resuspended fresh from a 50-μg vial in DMSO. The dye was then diluted to 50 μM Hank's balanced salt solution and added to cells on ice for 1 min before fixation.

Quantification

Intercellular area was defined as the total area between two cells along their lateral contact (perpendicular to the wound direction) at the edge or first interior layer of a wounded monolayer. The lateral contact length varied between 30 and 60 μm for both control and FMNL3-suppressed cells. Filopodia frequency was calculated from the number of filopodia that appeared in 25 min along a 50-μm length of protrusive cell edge, and filopodia lifetime was determined from frame-by-frame analysis of the movie files. For filopodia at cell–cell contacts, many lasted the length of the movie (~25 min) and thus were given that lifetime. Puncta diameter was measured using Nikon Elements software from 100×/1.4 NA images of fixed cells stained with anti-FMNL3. Because the puncta appeared circular by eye, the diameter was measured horizontally across each punctum. From this analysis, the mean punctual diameter is 370 ± 50 nm (n = 82), with no observed punctum being >540 in nm diameter. To quantify the expression level of FMNL3-NC-GFPint, we examined fixed cells by immunofluorescence microscopy, staining induced and uninduced cells with anti-FMNL3 and Alexa 546–labeled secondary antibody. Anti-FMNL3 recognizes both endogenous FMNL3 and FMNL3-NC-GFPint. We quantified total GFP and Alexa 546 fluorescence for each cell (normalizing both to cell area, and background subtracting from areas of the coverslip devoid of cells) and plotted total FMNL3 fluorescence (Alexa 546) as a function of GFP fluorescence. The resulting graph is shown in Supplemental Figure S4 and indicates that even the cells with highest FMNL3-NC-GFPint induction had no more than twofold increase in total FMNL3. The cells selected for

observation expressed significantly less GFP than the highest-expressing cells. Therefore, we conclude that the levels of FMNL3-NC-GFPint in our live-cell experiments were less than the level of endogenous FMNL3.

ACKNOWLEDGMENTS

We thank Ann Lavanway for lots of help with confocal microscopy; Bernardo Orr for guiding us through production of the Tet-On system; John Copeland for kind gifts of the FMNL3 ORF, FMNL2 expression plasmids, and anti-FMNL2 antibody; Brent Berwin for the labeled WGA; and Dan Hiose for just sticking with it on this project. This work was supported by National Institutes of Health Grant R01 GM069818, by American Recovery and Reinvestment Act funds under this grant, and by National Institutes of Health Grant S10RR024688 for purchase of the spinning disk confocal microscope.

REFERENCES

Adams CL, Chen YT, Smith SJ, Nelson WJ (1998). Mechanisms of epithelial cell-cell adhesion and cell compaction revealed by high-resolution tracking of E-cadherin-green fluorescent protein. J Cell Biol 142, 1105–1119.

Akhtar N, Hotchin NA (2001). RAC1 regulates adherens junctions through endocytosis of E-cadherin. Mol Biol Cell 12, 847–862.

Bai SW, Herrera-Abreu MT, Rohn JL, Racine V, Tajadura V, Suryavanshi N, Bechtel S, Wiemann S, Baum B, Ridley AJ (2011). Identification and characterization of a set of conserved and new regulators of cytoskeletal organization, cell morphology and migration. BMC Biol 9, 54.

Block J, Breitsprecher D, Kuhn S, Winterhoff M, Kage F, Geffers R, Duwe P, Rohn JL, Baum B, Brakebusch C, *et al*. (2012). FMNL2 drives actin-based protrusion and migration downstream of Cdc42. Curr Biol 22, 1005–1012.

Brevier J, Montero D, Svitkina T, Riveline D (2008). The asymmetric self-assembly mechanism of adherens junctions: a cellular push-pull unit. Phys Biol 5, 016005.

Campellone KG, Welch MD (2010). A nucleator arms race: cellular control of actin assembly. Nat Rev Mol Cell Biol 11, 237–251.

Colon-Franco JM, Gomez TS, Billadeau DD (2011). Dynamic remodeling of the actin cytoskeleton by FMNL1gamma is required for structural maintenance of the Golgi complex. J Cell Sci 124, 3118–3126.

Courtemanche N, Pollard TD (2012). Determinants of formin homology 1 (FH1) domain function in actin filament elongation by formins. J Biol Chem 287, 7812–7820.

Desclozeaux M, Venturato J, Wylie FG, Kay JG, Joseph SR, Le HT, Stow JL (2008). Active Rab11 and functional recycling endosome are required for E-cadherin trafficking and lumen formation during epithelial morphogenesis. Am J Physiol Cell Physiol 295, C545–C556.

Favaro P, Traina F, Machado-Neto JA, Lazarini M, Lopes MR, Pereira JK, Costa FF, Infante E, Ridley AJ, Saad ST (2013). FMNL1 promotes proliferation and migration of leukemia cells. J Leukocyte Biol 94, 503–512.

Gomez TS, Kumar K, Medeiros RB, Shimizu Y, Leibson PJ, Billadeau DD (2007). Formins regulate the actin-related protein 2/3 complex-independent polarization of the centrosome to the immunological synapse. Immunity 26, 177–190.

Han Y, Eppinger E, Schuster IG, Weigand LU, Liang X, Kremmer E, Peschel C, Krackhardt AM (2009). Formin-like 1 (FMNL1) is regulated by N-terminal myristoylation and induces polarized membrane blebbing. J Biol Chem 284, 33409–33417.

Harris ES, Gauvin TJ, Heimsath EG, Higgs HN (2010). Assembly of filopodia by the formin FRL2 (FMNL3). Cytoskeleton 67, 755–772.

Harris ES, Li F, Higgs HN (2004). The mouse formin, FRLa, slows actin filament barbed end elongation, competes with capping protein, accelerates polymerization from monomers, and severs filaments. J Biol Chem 279, 20076–20087.

Heimsath EG Jr, Higgs HN (2012). The C terminus of formin FMNL3 accelerates actin polymerization and contains a WH2 domain-like sequence that binds both monomers and filament barbed ends. J Biol Chem 287, 3087–3098.

Hetheridge C, Scott AN, Swain RK, Copeland JW, Higgs HN, Bicknell R, Mellor H (2012). The formin FMNL3 is a cytoskeletal regulator of angiogenesis. J Cell Sci 125, 1420–1428.

Higgs HN, Peterson KJ (2005). Phylogenetic analysis of the formin homology 2 domain. Mol Biol Cell 16, 1–13.

Hoelzle MK, Svitkina T (2012). The cytoskeletal mechanisms of cell-cell junction formation in endothelial cells. Mol Biol Cell 23, 310–323.

Kitzing TM, Wang Y, Pertz O, Copeland JW, Grosse R (2010). Formin-like 2 drives amoeboid invasive cell motility downstream of RhoC. Oncogene 29, 2441–2448.

Kovar DR, Sirotkin V, Lord M (2011). Three's company: the fission yeast actin cytoskeleton. Trends Cell Biol 21, 177–187.

Le TL, Yap AS, Stow JL (1999). Recycling of E-cadherin: a potential mechanism for regulating cadherin dynamics. J Cell Biol 146, 219–232.

Li Y, Zhu X, Zeng Y, Wang J, Zhang X, Ding YQ, Liang L (2010). FMNL2 enhances invasion of colorectal carcinoma by inducing epithelial-mesenchymal transition. Mol Cancer Res 8, 1579–1590.

Liang L, Li X, Zhang X, Lv Z, He G, Zhao W, Ren X, Li Y, Bian X, Liao W, *et al*. (2013). MicroRNA-137, an HMGA1 target, suppresses colorectal cancer cell invasion and metastasis in mice by directly targeting FMNL2. Gastroenterology 144, 624–635 e4.

Mersich AT, Miller MR, Chkourko H, Blystone SD (2010). The formin FRL1 (FMNL1) is an essential component of macrophage podosomes. Cytoskeleton 67, 573–585.

Moriya K, Yamamoto T, Takamitsu E, Matsunaga Y, Kimoto M, Fukushige D, Kimoto C, Suzuki T, Utsumi T (2012). Protein N-myristoylation is required for cellular morphological changes induced by two formin family proteins, FMNL2 and FMNL3. Biosci Biotechnol Biochem 76, 1201–1209.

Moseley JB, Goode BL (2006). The yeast actin cytoskeleton: from cellular function to biochemical mechanism. Microbiol Mol Biol Rev 70, 605–645.

Naj X, Hoffmann AK, Himmel M, Linder S (2013). The formins FMNL1 and mDia1 regulate coiling phagocytosis of Borrelia burgdorferi by primary human macrophages. Infect Immun 81, 1683–1695.

Palacios F, Tushir JS, Fujita Y, D'Souza-Schorey C (2005). Lysosomal targeting of E-cadherin: a unique mechanism for the down-regulation of cell-cell adhesion during epithelial to mesenchymal transitions. Mol Cell Biol 25, 389–402.

Paul AS, Pollard TD (2009). Review of the mechanism of processive actin filament elongation by formins. Cell Motil Cytoskeleton 66, 606–617.

Peglion F, Llense F, Etienne-Manneville S (2014). Adherens junction treadmilling during collective migration. Nat Cell Biol 16, 636–651.

Raub TJ, Koroly MJ, Roberts RM (1990). Rapid endocytosis and recycling of wheat germ agglutinin binding sites on CHO cells: evidence for two compartments in a nondegradative pathway. J Cell Physiol 144, 52–61.

Rosado M, Barber CF, Berciu C, Feldman S, Birren SJ, Nicastro D, Goode BL (2014). Critical roles for multiple formins during cardiac myofibril development and repair. Mol Biol Cell 25, 811–827.

Seth A, Otomo C, Rosen MK (2006). Autoinhibition regulates cellular localization and actin assembly activity of the diaphanous-related formins FRLalpha and mDia1. J Cell Biol 174, 701–713.

Trajkovic K, Hsu C, Chiantia S, Rajendran L, Wenzel D, Wieland F, Schwille P, Brügger B, Simons M (2008). Ceramide triggers budding of exosome vesicles into multivesicular endosomes. Science 319, 1244–1247.

Vaillant DC, Copeland SJ, Davis C, Thurston SF, Abdennur N, Copeland JW (2008). Interaction of the N- and C-terminal auto-regulatory domains of FRL2 does not inhibit FRL2 activity. J Biol Chem 283, 33750–33762 .

Vasioukhin V, Bauer C, Yin M, Fuchs E (2000). Directed actin polymerization is the driving force for epithelial cell-cell adhesion. Cell 100, 209–219.

Vega FM, Fruhwirth G, Ng T, Ridley AJ (2011). RhoA and RhoC have distinct roles in migration and invasion by acting through different targets. J Cell Biol 193, 655–665.

Zacharias DA, Violin JD, Newton AC, Tsien RY (2002). Partitioning of lipid-modified monomeric GFPs into membrane microdomains of live cells. Science 296, 913–916.

Zhu XL, Liang L, Ding YQ (2008). Overexpression of FMNL2 is closely related to metastasis of colorectal cancer. Int J Colorectal Dis 23, 1041–1047.

Zhu XL, Zeng YF, Guan J, Li YF, Deng YJ, Bian XW, Ding YQ, Liang L (2011). FMNL2 is a positive regulator of cell motility and metastasis in colorectal carcinoma. J Pathol 224, 377–388.